

RESEARCH ARTICLE | JULY 17 2024

Optical contrast analysis of α -RuCl₃ nanoflakes on oxidized silicon wafers

Tatyana V. Ivanova ; Daniel Andres-Penares ; Yiping Wang; Jiaqiang Yan; Daniel Forbes ; Servet Ozdemir ; Kenneth S. Burch; Brian D. Gerardot ; Mauro Brotons-Gisbert  



APL Mater. 12, 071114 (2024)

<https://doi.org/10.1063/5.0212132>

 CHORUS



Articles You May Be Interested In

Study of ruthenium behavior in alkali chloride melts using electronic absorption spectroscopy


AIP Conf. Proc. (December 2019)

The effect of number of nano structural coating containing Ti and Ru created by electro deposition

AIP Conf. Proc. (January 2018)

Thickness dependence of domain size in 2D ferroelectric CuInP₂S₆ nanoflakes

AIP Advances (November 2019)



Your One-Stop Shop for the Best Brands in Optics

- Extensive inventory with over 34,000 products available & 2,900 new products
- Fast shipping from our 9 distribution centres around the globe
- Bringing 80+ years of optical expertise to customers worldwide

Edmund
optics | worldwide

[Shop Now](#)

Optical contrast analysis of α -RuCl₃ nanoflakes on oxidized silicon wafers

Cite as: APL Mater. 12, 071114 (2024); doi: 10.1063/5.0212132

Submitted: 3 April 2024 • Accepted: 4 July 2024 •

Published Online: 17 July 2024



Tatyana V. Ivanova,¹ Daniel Andres-Penares,¹ Yiping Wang,² Jiaqiang Yan,³ Daniel Forbes,¹ Servet Ozdemir,^{1,a)} Kenneth S. Burch,² Brian D. Gerardot,¹ and Mauro Brotons-Gisbert^{1,b)}

AFFILIATIONS

¹ Institute of Photonics and Quantum Sciences, SUPA, Heriot-Watt University, Edinburgh EH14 4AS, United Kingdom

² Department of Physics, Boston College, Chestnut Hill, Massachusetts 02467, USA

³ Materials Science and Technology Division, Oak Ridge National Laboratory, Oak Ridge, Tennessee 37831, USA

^{a)} Current address: School of Physics and Astronomy, University of Leeds, Leeds LS2 9JT, United Kingdom.

^{b)} Author to whom correspondence should be addressed: m.brotons_i_gisbert@hw.ac.uk

ABSTRACT

α -RuCl₃, a narrow-band Mott insulator with a large work function, offers intriguing potential as a quantum material or as a charge acceptor for electrical contacts in van der Waals devices. In this work, we perform a systematic study of the optical reflection contrast of α -RuCl₃ nanoflakes on oxidized silicon wafers and estimate the accuracy of this imaging technique to assess the crystal thickness. Via spectroscopic micro-ellipsometry measurements, we characterize the wavelength-dependent complex refractive index of α -RuCl₃ nanoflakes of varying thickness in the visible and near-infrared. Building on these results, we simulate the optical contrast of α -RuCl₃ nanoflakes with thicknesses below 100 nm on SiO₂/Si substrates under different illumination conditions. We compare the simulated optical contrast with experimental values extracted from optical microscopy images and obtain good agreement. Finally, we show that optical contrast imaging allows us to retrieve the thickness of the RuCl₃ nanoflakes exfoliated on an oxidized silicon substrate with a mean deviation of -0.2 nm for thicknesses below 100 nm with a standard deviation of only 1 nm. Our results demonstrate that optical contrast can be used as a non-invasive, fast, and reliable technique to estimate the α -RuCl₃ thickness.

© 2024 Author(s). All article content, except where otherwise noted, is licensed under a Creative Commons Attribution (CC BY) license (<https://creativecommons.org/licenses/by/4.0/>). <https://doi.org/10.1063/5.0212132>

I. INTRODUCTION

van der Waals materials offer an unprecedented possibility to design and fabricate two-dimensional (2D) heterostructure devices due to the presence of a broad palette of atomically thin crystals with unique optical, electric, and magnetic properties. Among the different van der Waals layered crystals, the narrow-band Mott insulator α -RuCl₃ has emerged as a new building block for achieving local charge control in 2D van der Waals heterostructures. Its narrow electronic bands and large work function make α -RuCl₃ (hereafter RuCl₃) an excellent atomic crystalline charge acceptor, enabling modulation doping of several atomically thin crystals even when just a single RuCl₃ layer is employed.¹ Recently, RuCl₃ has been used to demonstrate low-resistance Ohmic contact for p-type WSe₂ at low temperatures and low carrier densities,^{2,3} overcoming the well-known challenges associated with achieving low-resistance electrical contacts in

monolayer transition-metal dichalcogenide semiconductors.^{4,5} Furthermore, the unique electronic structure of RuCl₃ itself has attracted a lot of attention due to its complex magnetic interactions, including access to a Kitaev quantum spin liquid phase.^{6–9} Combined, these properties position 2D RuCl₃ as a versatile building block in the van der Waals platform, with the potential to incorporate novel magnetic states¹⁰ and the resulting topological excitations into 2D devices.¹

Similar to other 2D materials, high quality RuCl₃ nanoflakes are usually obtained by mechanical exfoliation from bulk crystals on oxidized silicon wafers,¹¹ which typically results in stochastic nanoflakes with randomly varying thicknesses, lateral dimensions, and spatial locations on the substrate. In this context, an experimental technique that allows a fast, non-destructive, and accurate estimation of the thickness of the RuCl₃ nanoflakes would represent a valuable asset in the fabrication of 2D heterostructures incorporating this material. Although optical microscopy is routinely employed

as an initial step in the thickness estimation of mechanically exfoliated RuCl_3 ,^{3,12} to our knowledge, a systematic study of the optical reflection contrast of RuCl_3 nanoflakes on oxidized silicon wafers is still missing.

Here, we perform spectroscopic ellipsometry measurements at room temperature on mechanically exfoliated RuCl_3 nanoflakes of different thicknesses for photon wavelengths in the visible and near infrared range. Our measurements allow us to estimate the wavelength-dependent complex refractive index of RuCl_3 nanoflakes in this spectral range, confirming their thickness-independent optical properties. Building on these results, we exploit the estimated complex refractive index to calculate the optical contrast of RuCl_3 nanoflakes between ~ 2 and 100 nm on SiO_2/Si substrates under different illumination conditions. We compare the calculated optical contrast with the thickness-dependent experimental optical contrast extracted from optical microscopy images, showing good agreement between the simulated and experimental values. The good agreement between the calculated and experimental optical contrast allows us to predict the monochromatic illumination wavelengths that maximize the optical contrast response of RuCl_3 nanoflakes below 10 nm for two standard thicknesses (90 and 295 nm) of the SiO_2 layer on a Si substrate. Finally, we show that for RuCl_3 nanoflakes in the range 2 – 100 nm imaged with our calibrated standard optical microscope, the crystal thickness estimated exclusively from the optical contrast analysis shows only a mean deviation of -0.2 nm from the value measured by a combination of atomic force microscopy (AFM) and spectroscopic ellipsometry, with a standard deviation close to the thickness of a single RuCl_3 monolayer. Our results provide valuable information about the optical properties of 2D RuCl_3 flakes in the visible and near infrared, which are crucial in exploiting this material in 2D nanodevices. Moreover, we show that optical contrast can be used as a non-invasive, fast, and reliable technique to estimate RuCl_3 crystal thicknesses.

II. COMPLEX REFRACTIVE INDEX OF RuCl_3 IN THE VISIBLE AND NEAR-INFRARED

We begin by performing spectroscopic micro-ellipsometry measurements at room temperature on RuCl_3 nanoflakes with thicknesses between ~ 3 and 40 nm for photon wavelengths in the visible and near infrared (~ 1.4 – 3.1 eV). The RuCl_3 nanoflakes were obtained by mechanical exfoliation from bulk crystals directly on Si substrates with a top SiO_2 layer with a nominal thickness of 295 nm. The thickness of each nanoflake was measured by AFM. The spectroscopic micro-ellipsometry measurements were carried out using an Accurion EP4 imaging ellipsometer with a spatial resolution of ~ 1 μm . Figure 1(a) shows a sketch of the experimental measurement setup. The ellipsometric Δ and Ψ angles of the multilayer system ($\text{RuCl}_3/\text{SiO}_2/\text{Si}$) were measured as a function of the energy and the angle of incidence (AOI) of the illumination light. Figure 1(b) shows the Δ (red) and Ψ (blue) angles measured under AOIs of 45° (filled circles) and 50° (empty circles) for RuCl_3 nanoflakes with thicknesses of 2.9 , 6.9 , and 36.5 nm. We note that these measurements were repeated for different in-plane rotations of the RuCl_3 samples, leading to imperceptible differences in the measured Δ and Ψ angles, as expected from the in-plane isotropic optical response of the material. Moreover, with the aim of minimizing

substrate-induced uncertainties in the determination of the refractive index of RuCl_3 nanoflakes, ellipsometric angles from the bare SiO_2/Si substrate were also measured simultaneously on spatial positions a few micrometers away from each RuCl_3 nanoflake using the same experimental conditions.

For a quantitative analysis of the optical properties of the RuCl_3 nanoflakes, it is necessary to fit the measured ellipsometry angles with simulated data from an optical model of the corresponding multilayer sample. To build the optical model of the sample, we use the analysis software of the Accurion EP4 ellipsometer (EP4Model), which calculates the normalized Mueller matrix describing the polarizing properties for reflection and transmission of layered thin-film samples.^{13–15} In the first step of our analysis, we fit the experimental ellipsometry data measured on the bare substrate to a multilayer model consisting of a SiO_2 layer on top of a semi-infinite silicon substrate using the reported refractive indices for Si and SiO_2 .¹⁶ The Levenberg–Marquardt-algorithm fit engine of the EP4Model software yields a thickness of 295 ± 0.2 nm for the SiO_2 layer. In the next step of our analysis, we build a new multilayer model consisting of a RuCl_3 layer of unknown complex refractive index on top of a 295 -nm-thick SiO_2 layer above a semi-infinite silicon substrate and use it to fit simultaneously the experimental Δ and Ψ angles for different crystal thicknesses and angles of incidence shown in Fig. 1(b). Figure 1(c) shows the estimated complex refractive index of RuCl_3 obtained from the simultaneous fit of the six experimental datasets in Fig. 1(b). The solid lines in Fig. 1(b) show the modeled ellipsometric Δ and Ψ angles obtained using the refractive index shown in Fig. 1(c). As can be observed, the calculated Δ and Ψ angles agree very well with the experimental data obtained from flakes with thicknesses of 2.9 , 6.9 , and 36.5 nm, confirming the thickness-independent optical properties of this material.

Furthermore, we observe a very good agreement between the estimated refractive index of the nanoflakes and the optical properties reported for bulk RuCl_3 crystals in previous studies.^{17–20} As shown in Fig. 1(c), the imaginary part of the refractive index (κ) shows a clear absorption peak at ~ 2.05 eV, in good agreement with the β resonance reported in the imaginary part of the dielectric constant¹⁹ and the real part of the optical conductivity of bulk RuCl_3 crystals.²⁰ The observed increase of κ toward the edges of our measurement range also agrees well with the reported existence of stronger α and γ absorption resonances at ~ 1.2 and 3.2 eV, respectively.^{19,20}

III. OPTICAL CONTRAST ANALYSIS OF RuCl_3

Next, we employ the measured complex refractive index of RuCl_3 to calculate its thickness-dependent optical contrast when deposited on top of SiO_2/Si substrates and imaged with an optical microscope in an epi-illumination configuration. In our simulations, we adopt the following definition for the optical contrast between the nanoflake and the substrate:^{21,22} $OC(\lambda) = (R(\lambda) - R_0(\lambda)) / (R(\lambda) + R_0(\lambda))$, where $R(\lambda)$ and $R_0(\lambda)$ represent the wavelength-dependent intensities of the light reflected by the whole heterostack ($\text{RuCl}_3/\text{SiO}_2/\text{Si}$) and the bare substrate (SiO_2/Si), respectively. To calculate $R(\lambda)$ and $R_0(\lambda)$, we employ the transfer matrix method, in which the forward- and backward-propagating plane waves form the basis into which the optical electric field

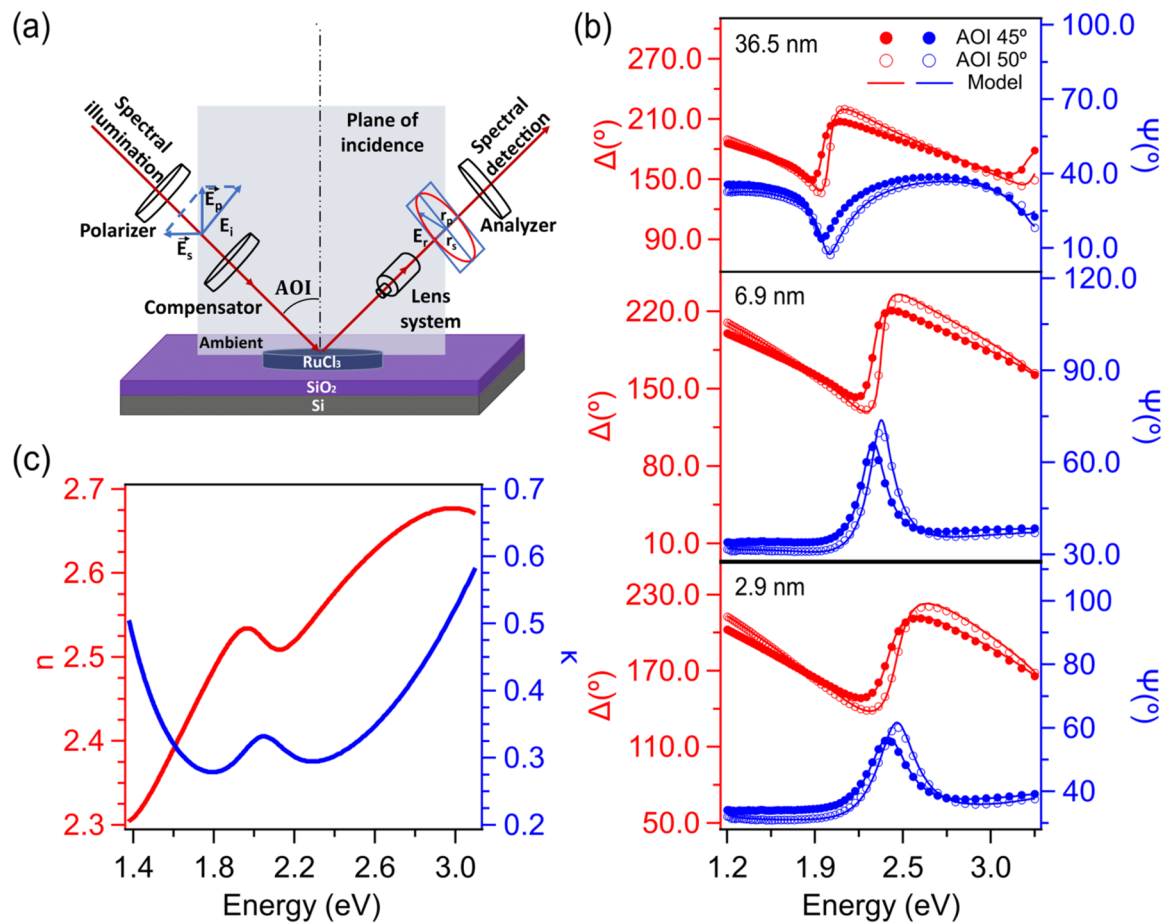


FIG. 1. (a) Schematic representation of the experimental spectroscopic ellipsometry setup. (b) Δ (red) and Ψ (blue) ellipsometric angles measured under AOIs of 45° (filled circles) and 50° (empty circles) for RuCl₃ nanoflakes with thicknesses of 2.9 (bottom), 6.9 (middle), and 36.5 nm (top). The solid lines represent the fit of the experimental data using a Mueller matrix formalism. (c) Estimated complex refractive index of RuCl₃ obtained from a simultaneous fitting of the Δ and Ψ angles shown in (b) for different crystal thicknesses.

in each layer is decomposed.²³ In our simulations, we include the wavelength-dependent refractive indices of SiO₂ and Si¹⁶ and assume a normal incidence of illumination for simplicity. Although the angular spread of incident angles given by the numerical aperture (NA) of the illumination objective lens can play a significant role in the perceived optical contrast for thick crystals and/or 2D layers with anisotropic optical constants,^{24,25} the relatively thin flakes (<100 nm), the low NA of the objective lens (0.42), and the measured isotropic refractive index of RuCl₃ justify our assumption.

A. Thickness-dependent optical contrast of RuCl₃ in the sRGB color space

In this section, we explore experimentally and numerically the thickness-dependent optical contrast of RuCl₃ on SiO₂/Si substrates in the standard RGB (sRGB) color space under broadband white illumination. Figure 2(a) shows an optical microscope image in the sRGB color space of RuCl₃ flakes with thicknesses in the

range ~2–100 nm mechanically exfoliated on a SiO₂/Si substrate with a SiO₂ thickness of 295 nm, as confirmed by spectroscopic ellipsometry. The red, green, and blue dots in Fig. 2(b) represent the experimental optical contrast values in the different channels (R, G, and B, respectively) extracted from the optical microscope image shown in Fig. 2(a) and a second spot nearby on the same substrate. The thicknesses of the layers indicated in Fig. 2 were estimated by a combination of AFM and spectroscopic ellipsometry measurements, while the optical contrast values and corresponding error bars represent the optical contrast value and associated uncertainty calculated from the measured $R(\lambda)$ and $R_0(\lambda)$ in each flake and a nearby spot in the substrate, respectively. The experimental values and uncertainties of $R(\lambda)$ and $R_0(\lambda)$ for all the measured flakes were obtained from the median and standard deviation, respectively, of 100 pixels.

In order to compare the experimental contrast values in the sRGB color space with the calculated optical contrast, we follow the approach described in previous studies.^{16,26–29} In this approach,

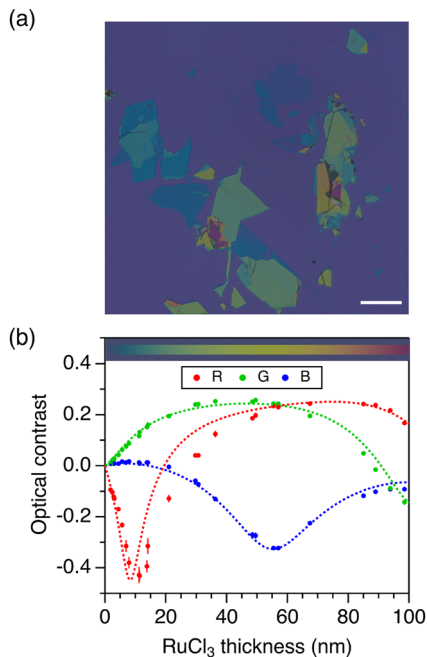


FIG. 2. (a) Optical microscope image, acquired in the standard RGB (sRGB) color space, of exfoliated RuCl_3 flakes with thicknesses ranging from ~ 2 to 100 nm. Scale bar: 50 μm . (b) Comparison of the experimental (dots) and calculated (dashed lines) optical contrast in the sRGB color space corresponding to the red (R), green (G), and blue (B) channels. The colorscale bar shows the calculated color of RuCl_3 as a function of flake thickness when deposited on top of a SiO_2/Si substrate with a SiO_2 thickness of 295.5 nm.

the simulated wavelength-dependent reflected intensities of the flake and bare substrate ($R(\lambda)$ and $R_0(\lambda)$) are used to calculate CIE XYZ color values, which simulate the color perceived by the human eye. Such transformation involves integration over wavelengths, including the light source spectrum (Thorlabs, Inc., product MCWHL P1) and the CIE color-matching functions to calculate the XYZ tristimulus components.^{16,26,27} Finally, the calculated XYZ values are converted to the sRGB color space using a standard transformation, which takes into account the chromaticity coordinates of the sRGB color space and the reference white of the light source.^{16,30}

The dashed lines in Fig. 2(b) show sRGB optical contrast values for the R, G, and B channels as a function of flake thickness calculated following the approach described above. We note that in order to get a good agreement with the experimental values, the simulated optical contrast response of the three channels must be scaled by a normalization factor f (with $f < 1$). We justify the use of such a normalization factor by the need to account for the reduced spatial and temporal coherence of the illumination light in our experimental setup (which we assume to be perfect in the simulations), which is known to result in reduced visibility of the interference fringes in the reflected signals while preserving the thickness-dependent positions of the interference maxima and minima.³¹ We find that a normalization factor $f = 0.68$ effectively reproduces the observed optical contrast in all three RGB channels for all measured RuCl_3 thicknesses. Notably, the best agreement is found using the G and

B channels, showing goodness-of-fit parameters (GoF) > 0.98 , as compared to a value of ≈ 0.92 obtained for the R channel, where $\text{GoF} = 1 - \text{RMSE}$, with RMSE being the root-mean-square error.

The good agreement between the experimental and simulated optical contrast allows us to calculate the apparent color of RuCl_3 on a $\text{SiO}_2(295 \text{ nm})/\text{Si}$ substrate as a function of flake thickness. The colorbar on the top side of Fig. 2(b) shows the calculated apparent colors of the substrate (outer region) and the RuCl_3 (inner region) as a function of thickness. Overall, we find a good agreement between the measured and calculated apparent color of RuCl_3 , which can be used as a fast method for assessing flake thicknesses, as shown previously for other different 2D materials.^{27,29,32,33}

B. Thickness-dependent optical contrast of RuCl_3 under narrow-band illumination

Next, we explore the effects that the inclusion of narrow optical bandpass filters in the illumination path has on the optical contrast characterization of RuCl_3 . This approach has previously been shown to reproduce, to a good extent, the optical contrast simulated under monochromatic illumination in other 2D crystals.^{22,34–36} The blue and red dots in Fig. 3(a) represent the experimental contrast values measured for the same RuCl_3 flakes shown in Fig. 2 when filtering the illumination spectrum with 10-nm-bandwidth filters centered at 450 and 600 nm, respectively. The blue and red dashed lines indicate the simulated thickness-dependent evolution of the optical contrast

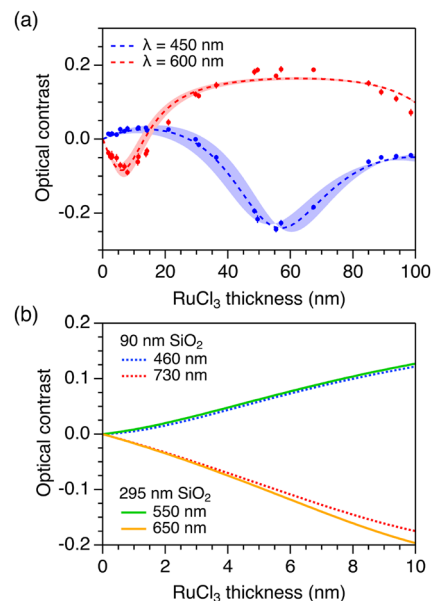


FIG. 3. (a) Comparison of the experimental (dots) and calculated (dashed lines) optical contrast of RuCl_3 with thicknesses ~ 2 –100 nm measured using bandpass filters at 450 nm (blue) and 600 nm (red) with a 10-nm bandwidth. The shaded areas represent the calculated optical contrast at the corresponding central wavelength of the filter, ± 5 nm. (b) Calculated optical contrast under the monochromatic excitation wavelengths that maximize the positive and negative optical contrast of RuCl_3 with thicknesses in the range ~ 0 –10 nm for SiO_2 thicknesses of 90 nm (dashed lines) and 295 nm (solid lines).

assuming monochromatic excitation at 450 and 600 nm, respectively. The blue and red shaded areas show the simulated optical contrast for monochromatic illumination in the ranges of 450 ± 5 and 600 ± 5 nm, respectively. Similar to the results under broadband illumination, we observe that the simulated optical contrast agrees well with the experimental values across the whole thickness range. Again, we find a better agreement between simulated and experimental values for the shorter illumination wavelength, with GoF values of 0.99 and 0.98 for the 450 and 600 nm filters, respectively.

Once more, the good agreement between the optical contrast measured with bandpass filters and the simulated optical contrast under monochromatic illumination allows us to explore the monochromatic wavelengths that enhance the optical contrast response of RuCl_3 with thicknesses below 10 nm on top of Si substrates with thermally grown SiO_2 layers. Note that an enhanced optical contrast response arises from a combination of large absolute optical contrast with the underlying substrate and a linear dependence on RuCl_3 thickness. Figure 3(b) summarizes the results of our analysis for two standard SiO_2 thicknesses of 90 and 295 nm. Our results suggest that monochromatic illumination wavelengths of ~ 730 and ~ 650 nm yield the largest optical contrast values for 90 and 295-nm-thick SiO_2 layers, respectively, while showing an almost linear dependence with RuCl_3 thickness in the explored range. We note that in both cases, the optimized monochromatic illumination wavelengths result in a negative optical contrast, i.e., the RuCl_3 crystal appears darker than the substrate. We find that monochromatic illumination wavelengths of ~ 460 and ~ 550 nm give rise to the opposite case (i.e., RuCl_3 appears brighter than the substrate) for 90 and 295-nm-thick SiO_2 layers, respectively, at the expense of a slightly lower absolute optical contrast.

C. RuCl_3 thickness estimation from optical contrast measurements

Finally, in this section, we benchmark the performance of the optical contrast technique to estimate the thickness of RuCl_3 nanoflakes using our calibrated optical microscope and the experimental optical contrast dataset shown in Figs. 2 and 3. In order to do so, we employ an algorithm that estimates the value of the RuCl_3 thickness (d) and minimizes the following quantity:

$$RMSE^{total}(d) = \sqrt{\sum_i^N \frac{[OC_{exp}^i - OC_{sim}^i(d)]^2}{N}}, \quad (1)$$

with N representing the total number of experimental and simulated optical contrast illumination/detection modes i considered for the minimization algorithm (i.e., sRGB detection for white illumination or bandpass illumination). In our algorithm, we follow a two-step approach. We start by considering only the two optical contrast configurations that show the best overall agreement between experimental and simulated values (G and B channel detection under broadband illumination) and estimate the crystal thickness (d) that minimizes Eq. (1). In the second step, if the value of d returned by the initial minimization of Eq. (1) for the G and B channels falls outside the range $3.5 \leq d \leq 55$ nm (i.e., where the R channel shows a good agreement between experiment and simulations), we minimize again Eq. (1) with the addition of the R channel. This

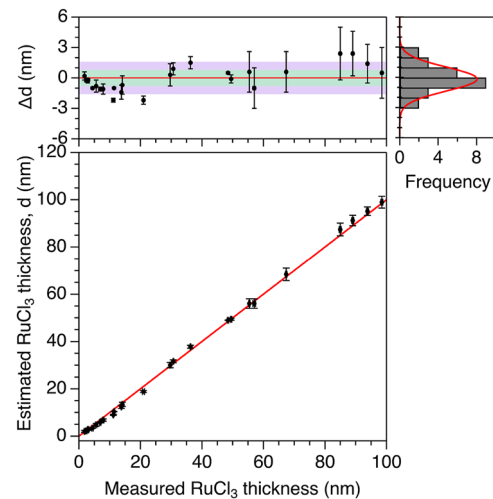


FIG. 4. Bottom panel: RuCl_3 thickness estimated from the experimental optical contrast obtained by a combination of sRGB and monochromatic detection as a function of the thickness determined by independent AFM and/or spectroscopic ellipsometry measurements. The horizontal error bars represent the uncertainty associated with the independent thickness estimation. The vertical error bars represent the uncertainty resulting from our thickness estimation approach, which we define as the thickness range for which the $RMSE^{total}$ defined by Eq. (1) is less than or equal to two times the $RMSE^{total}$ corresponding to the estimated thickness. The red line represents the ideal case, where the thickness inferred from the optical contrast equals the measured thickness. Top panel: difference between the estimated thickness inferred from the optical contrast and the measured RuCl_3 thickness (Δd). The green and purple shaded areas represent Δd intervals of ± 1 and ± 2 RuCl_3 monolayers, respectively. The histogram in the top-right panel identifies the statistics using monolayer thickness binning.

two-step minimization procedure results in an estimated thickness with a mean deviation $\overline{\Delta d} = -0.2$ nm from the crystal thickness estimated by AFM/ellipsometry in the range $d < 100$ nm with a standard deviation of 1.2 nm.

Finally, we note that the inclusion of an additional measurement mode (450 nm band-pass detection) in the second stage of the two-step minimization algorithm leads to a slight improvement in the thickness estimation performance. The bottom panel of Fig. 4 shows the RuCl_3 thickness estimated from the experimental optical contrast as a function of the thickness determined by AFM and spectroscopic ellipsometry measurements. The red line represents the ideal case, where the thickness inferred from the optical contrast equals the measured thickness. The top panel shows the difference between the estimated thickness inferred from the optical contrast and the measured RuCl_3 thickness (Δd), with the green and purple shaded areas representing Δd intervals of ± 1 and ± 2 RuCl_3 monolayers, respectively. Finally, the top right panel shows a histogram of the corresponding Δd values, which yields a $\overline{\Delta d} = -0.2$ nm for the whole thickness range with a standard deviation of 1 nm, i.e., close to the thickness of a single RuCl_3 monolayer (0.8 nm^{37,38}).

IV. CONCLUSIONS

In summary, we report the complex refractive index of α - RuCl_3 nanoflakes with thicknesses below 40 nm in the visible

and near-infrared wavelength ranges. Our results show that the optical properties of the nanoflakes are independent of the crystal thickness and agree well with the optical constants reported for bulk samples.^{17–20} Compared to other 2D crystals such as transition-metal dichalcogenide semiconductors,³⁹ group III–VI metal chalcogenide semiconductors such as InSe,⁴⁰ or hybrid perovskites,⁴¹ which show strong modulation of their dielectric response with the thickness for few-layer crystals, the thickness-independent optical response of RuCl₃ enables a straightforward and reliable comparison between the experimental and simulated optical reflectance contrast as a function of crystal thickness. In this context, we show that transfer-matrix based simulations of the thickness-dependent optical contrast of RuCl₃ on oxidized silicon substrates reproduce with good agreement the experimental optical contrast obtained under different illumination/detection configurations, including sRGB color-space detection for broadband and narrow-band illumination. Finally, we show that optical contrast imaging allows us to retrieve the thickness of the RuCl₃ nanoflakes exfoliated on an oxidized silicon substrate with a mean deviation of -0.2 nm for thicknesses below 100 nm and a standard deviation of only 1 nm across the whole thickness range. These results demonstrate the potential of optical contrast analysis as a non-invasive, fast, and reliable technique to estimate the thickness of RuCl₃ nanoflakes.

ACKNOWLEDGMENTS

This work was supported by the EPSRC (Grant Nos. EP/P029892/1 and EP/L015110/1) and the ERC (Grant No. 725920) (D.A.-P., S. O., and B.D.G.). The work of Y.W. and K.S.B. was supported by the National Science Foundation (NSF) EPMD program via Grant No. EPMD-2211334. Crystal growth at ORNL was supported by the U.S. Department of Energy, Office of Science, National Quantum Information Science Research Centers, and Quantum Science Center. M.B.-G. is supported by a Royal Society University Research Fellowship. B.D.G. is supported by a Chair in Emerging Technology from the Royal Academy of Engineering.

AUTHOR DECLARATIONS

Conflict of Interest

The authors have no conflicts to disclose.

Author Contributions

T.V.I. and D.A.-P. contributed equally to this work.

Tatyana V. Ivanova: Conceptualization (equal); Formal analysis (equal); Investigation (lead); Writing – original draft (equal); Writing – review & editing (equal). **Daniel Andres-Penares:** Conceptualization (equal); Investigation (equal); Writing – review & editing (equal). **Yiping Wang:** Resources (supporting); Writing – review & editing (equal). **Jiaqiang Yan:** Resources (supporting); Writing – review & editing (equal). **Daniel Forbes:** Formal analysis (supporting); Investigation (supporting); Writing – review & editing (equal). **Servet Ozdemir:** Investigation (supporting); Writing –

review & editing (equal). **Kenneth S. Burch:** Resources (supporting); Writing – review & editing (equal). **Brian D. Gerardot:** Conceptualization (equal); Funding acquisition (equal); Resources (equal); Writing – original draft (equal); Writing – review & editing (equal). **Mauro Brotons-Gisbert:** Conceptualization (equal); Formal analysis (equal); Funding acquisition (equal); Resources (equal); Supervision (lead); Writing – original draft (equal); Writing – review & editing (equal).

DATA AVAILABILITY

The dataset generated and analyzed during the current study is available at <https://researchportal.hw.ac.uk/en/persons/mauro-brotons-i-gisbert/datasets/>

REFERENCES

- Y. Wang, J. Balgley, E. Gerber, M. Gray, N. Kumar, X. Lu, J.-Q. Yan, A. Feridouni, R. Basnet, S. J. Yun *et al.*, “Modulation doping via a two-dimensional atomic crystalline acceptor,” *Nano Lett.* **20**, 8446–8452 (2020).
- J. Pack, Y. Guo, Z. Liu, B. S. Jessen, L. Holtzman, S. Liu, M. Cothrine, K. Watanabe, T. Taniguchi, D. G. Mandrus *et al.*, “Charge-transfer contact to a high-mobility monolayer semiconductor,” *arXiv:2310.19782* (2023).
- J. Xie, Z. Zhang, H. Zhang, V. Nagarajan, W. Zhao, H. Kim, C. Sanborn, R. Qi, S. Chen, S. Kahn *et al.*, “Low resistance contact to P-type monolayer WSe₂,” *Nano Lett.* **24**, 5937–5943 (2024).
- A. Allain, J. Kang, K. Banerjee, and A. Kis, “Electrical contacts to two-dimensional semiconductors,” *Nat. Mater.* **14**, 1195–1205 (2015).
- Y. Wang and M. Chhowalla, “Making clean electrical contacts on 2D transition metal dichalcogenides,” *Nat. Rev. Phys.* **4**, 101–112 (2022).
- A. Banerjee, C. Bridges, J.-Q. Yan, A. Aczel, L. Li, M. Stone, G. Granroth, M. Lumsden, Y. Yiu, J. Knolle *et al.*, “Proximate Kitaev quantum spin liquid behaviour in a honeycomb magnet,” *Nat. Mater.* **15**, 733–740 (2016).
- A. Banerjee, J. Yan, J. Knolle, C. A. Bridges, M. B. Stone, M. D. Lumsden, D. G. Mandrus, D. A. Tennant, R. Moessner, and S. E. Nagler, “Neutron scattering in the proximate quantum spin liquid α -RuCl₃,” *Science* **356**, 1055–1059 (2017).
- S.-H. Do, S.-Y. Park, J. Yoshitake, J. Nasu, Y. Motome, Y. S. Kwon, D. Adroja, D. Voneshen, K. Kim, T.-H. Jang *et al.*, “Majorana fermions in the Kitaev quantum spin system α -RuCl₃,” *Nat. Phys.* **13**, 1079–1084 (2017).
- Y. Wang, G. B. Osterhoudt, Y. Tian, P. Lampen-Kelley, A. Banerjee, T. Goldstein, J. Yan, J. Knolle, H. Ji, R. J. Cava *et al.*, “The range of non-Kitaev terms and fractional particles in α -RuCl₃,” *npj Quantum Mater.* **5**, 14 (2020).
- W.-C. Lee and A. MacDonald, “Modulation doping near Mott-insulator heterojunctions,” *Phys. Rev. B* **74**, 075106 (2006).
- K. S. Novoselov, D. Jiang, F. Schedin, T. J. Booth, V. V. Khotkevich, S. V. Morozov, and A. K. Geim, “Two-dimensional atomic crystals,” *Proc. Natl. Acad. Sci. U. S. A.* **102**, 10451–10453 (2005).
- B. Yang, Y. M. Goh, S. H. Sung, G. Ye, S. Biswas, D. A. Kaib, R. Dhakal, S. Yan, C. Li, S. Jiang *et al.*, “Magnetic anisotropy reversal driven by structural symmetry-breaking in monolayer α -RuCl₃,” *Nat. Mater.* **22**, 50–57 (2023).
- H. Fujiwara, *Spectroscopic Ellipsometry: Principles and Applications* (John Wiley & Sons, 2007).
- H. G. Tompkins and J. N. Hilfiker, *Spectroscopic Ellipsometry: Practical Application to Thin Film Characterization* (Momentum Press, 2015).
- O. Arteaga and B. Kahr, “Characterization of homogenous depolarizing media based on mueller matrix differential decomposition,” *Opt. Lett.* **38**, 1134–1136 (2013).
- J. Henrie, S. Kellis, S. M. Schultz, and A. Hawkins, “Electronic color charts for dielectric films on silicon,” *Opt. Express* **12**, 1464–1469 (2004).
- L. Binotto, I. Pollini, and G. Spinolo, “Optical and transport properties of the magnetic semiconductor α -RuCl₃,” *Phys. Status Solidi B* **44**, 245–252 (1971).

- ¹⁸K. Plumb, J. Clancy, L. Sandilands, V. V. Shankar, Y. Hu, K. Burch, H.-Y. Kee, and Y.-J. Kim, “ α -RuCl₃: A spin-orbit assisted Mott insulator on a honeycomb lattice,” *Phys. Rev. B* **90**, 041112 (2014).
- ¹⁹L. J. Sandilands, Y. Tian, A. A. Reijnders, H.-S. Kim, K. W. Plumb, Y.-J. Kim, H.-Y. Kee, and K. S. Burch, “Spin-orbit excitations and electronic structure of the putative Kitaev magnet α -RuCl₃,” *Phys. Rev. B* **93**, 075144 (2016).
- ²⁰L. J. Sandilands, C. H. Sohn, H. J. Park, S. Y. Kim, K. W. Kim, J. A. Sears, Y.-J. Kim, and T. W. Noh, “Optical probe of Heisenberg-Kitaev magnetism in α -RuCl₃,” *Phys. Rev. B* **94**, 195156 (2016).
- ²¹I. Jung, M. Pelton, R. Piner, D. A. Dikin, S. Stankovich, S. Watcharotone, M. Hausner, and R. S. Ruoff, “Simple approach for high-contrast optical imaging and characterization of graphene-based sheets,” *Nano Lett.* **7**, 3569–3575 (2007).
- ²²A. Castellanos-Gomez, N. Agrait, and G. Rubio-Bollinger, “Optical identification of atomically thin dichalcogenide crystals,” *Appl. Phys. Lett.* **96**, 213116 (2010).
- ²³H. Macleod, *Thin-Film Optical Filters* (CRC Press, 2001).
- ²⁴J. M. Katzen, M. Velický, Y. Huang, S. Drakeley, W. Hendren, R. M. Bowman, Q. Cai, Y. Chen, L. H. Li, and F. Huang, “Rigorous and accurate contrast spectroscopy for ultimate thickness determination of micrometer-sized graphene on gold and molecular sensing,” *ACS Appl. Mater. Interfaces* **10**, 22520–22528 (2018).
- ²⁵F. Huang, “Optical contrast of atomically thin films,” *J. Phys. Chem. C* **123**, 7440–7446 (2019).
- ²⁶L. Gao, W. Ren, F. Li, and H.-M. Cheng, “Total color difference for rapid and accurate identification of graphene,” *ACS Nano* **2**, 1625–1633 (2008).
- ²⁷M. Müller, A. Gumplich, E. Ecik, K. Kallis, F. Winkler, B. Kardynal, I. Petrov, U. Kunze, and J. Knoch, “Visibility of two-dimensional layered materials on various substrates,” *J. Appl. Phys.* **118**, 145305 (2015).
- ²⁸M. Spina, C. Grimaldi, B. Náfrádi, L. Forró, and E. Horvath, “Rapid thickness reading of CH₃NH₃PbI₃ nanowire thin films from color maps,” *Phys. Status Solidi A* **213**, 2017–2023 (2016).
- ²⁹H. Chen, W. Fei, J. Zhou, C. Miao, and W. Guo, “Layer identification of colorful black phosphorus,” *Small* **13**, 1602336 (2017).
- ³⁰B. J. Lindbloom, “RGB/XYZ matrices,” http://www.bruceindbloom.com/index.html?Eqn_RGB_XYZ_Matrix.html (accessed January 2023).
- ³¹M. C. Tropicovsky, A. S. Sabau, A. R. Lupini, and Z. Zhang, “Transfer-matrix formalism for the calculation of optical response in multilayer systems: From coherent to incoherent interference,” *Opt. Express* **18**, 24715–24721 (2010).
- ³²S. Roddaro, P. Pingue, V. Piazza, V. Pellegrini, and F. Beltram, “The optical visibility of graphene: Interference colors of ultrathin graphite on SiO₂,” *Nano Lett.* **7**, 2707–2710 (2007).
- ³³S. Puebla, H. Li, H. Zhang, and A. Castellanos-Gomez, “Apparent colors of 2D materials,” *Adv. Photonics Res.* **3**, 2100221 (2022).
- ³⁴P. Blake, E. Hill, A. Castro Neto, K. Novoselov, D. Jiang, R. Yang, T. Booth, and A. Geim, “Making graphene visible,” *Appl. Phys. Lett.* **91**, 063124 (2007).
- ³⁵M. Brotons-Gisbert, D. Andres-Penares, J. Martínez-Pastor, A. Cros, and J. Sánchez-Royo, “Optical contrast of 2D InSe on SiO₂/Si and transparent substrates using bandpass filters,” *Nanotechnology* **28**, 115706 (2017).
- ³⁶M. Krečmarová, D. Andres-Penares, L. Fekete, P. Ashcheulov, A. Molina-Sánchez, R. Canet-Albiach, I. Gregora, V. Mortet, J. P. Martínez-Pastor, and J. F. Sánchez-Royo, “Optical contrast and Raman spectroscopy techniques applied to few-layer 2D hexagonal boron nitride,” *Nanomaterials* **9**, 1047 (2019).
- ³⁷B. Zhou, Y. Wang, G. B. Osterhoudt, P. Lampen-Kelley, D. Mandrus, R. He, K. S. Burch, and E. A. Henriksen, “Possible structural transformation and enhanced magnetic fluctuations in exfoliated α -RuCl₃,” *J. Phys. Chem. Solids* **128**, 291–295 (2019).
- ³⁸J.-H. Lee, Y. Choi, S.-H. Do, B. H. Kim, M.-J. Seong, and K.-Y. Choi, “Multiple spin-orbit excitons in α -RuCl₃ from bulk to atomically thin layers,” *npj Quantum Mater.* **6**, 43 (2021).
- ³⁹C. Hsu, R. Frisenda, R. Schmidt, A. Arora, S. M. De Vasconcellos, R. Bratschkitsch, H. S. van der Zant, and A. Castellanos-Gomez, “Thickness-dependent refractive index of 1L, 2L, and 3L MoS₂, MoSe₂, WS₂, and WSe₂,” *Adv. Opt. Mater.* **7**, 1900239 (2019).
- ⁴⁰M. Brotons-Gisbert, D. Andres-Penares, J. Suh, F. Hidalgo, R. Abargues, P. J. Rodriguez-Canto, A. Segura, A. Cros, G. Tobias, E. Canadell *et al.*, “Nanotexturing to enhance photoluminescent response of atomically thin indium selenide with highly tunable band gap,” *Nano Lett.* **16**, 3221–3229 (2016).
- ⁴¹B. Song, J. Hou, H. Wang, S. Sidhik, J. Miao, H. Gu, H. Zhang, S. Liu, Z. Fakhraei, J. Even *et al.*, “Determination of dielectric functions and exciton oscillator strength of two-dimensional hybrid perovskites,” *ACS Mater. Lett.* **3**, 148–159 (2020).